Border-collision bifurcation in the Logistic map with state-dependent impulsive forces

Haibo Jiang[1]*, Yang Liu[2], Liping Zhang[1], Jianjiang Yu[3]

[1]School of Mathematics and Statistics, Yancheng Teachers University, Yancheng 224002, China

[2]Exeter Small-Scale Robotics Laboratory, Engineering Department, University of Exeter, Exeter EX4 4QF, UK

[3]School of Information Engineering, Yancheng Teachers University, Yancheng 224002, China

ABSTRACT. This paper examines the intricate dynamics of the Logistic map involving impulsive forces that depend on the state. The conditions of stability and border-collision bifurcation (BCB) of periodic orbits are presented. The two-parameter dynamical regions and the two-parameter bifurcation diagram of the system with respect to the system parameter and the strength of impulsive force are constructed. The periodic tongues are given to show that the BCB is critical for the dynamics of the Logistic map with state-dependent impulsive forces. Finally, the bifurcation curves are provided to disclose the mechanisms of several bifurcation scenarios closely related to the BCB, including the period increment scenario and the period-adding scenario.

1. Introduction

State hopping of a system due to external perturbation is common in nature [1, 2]. For such a perturbation, it is usually assumed to be applied abruptly in the form of impulse [3]. Impulsive perturbation could degrade system performance and severely cause the system to lose stability. Therefore, the stability analysis and the controller synthesis problems of these systems have drawn considerable attention from researchers (see, e.g., [4]). In particular, the dynamical behaviors of continuous systems with periodic impulsive forces [5] or state-dependent impulsive forces [6] have been studied extensively. On the other hand, considerable attention has been devoted to studying the behavior of discrete systems that expe-

*This paper is submitted to the special issue "On Modeling, Analysis and Synthesis of Nonsmooth Dynamical Systems" of the journal "Discrete and Continuous Dynamical Systems Series S" for publication. 2020 Mathematics Subject Classification. Primary: 39A28; Secondary: 93C27. Key words and phrases. Logistic map, impulse, periodic orbit, border-collision bifurcation, period-adding scenario. This work is partially supported by the Fundamental Science (Natural Science) Foundation of the Jiangsu Higher Education Institutions of China (Grant No. 23KJA120004). Corresponding author: Haibo Jiang.

rience periodic impulsive forces due to their wide range of applications, including biology and internet congestion control, e.g., [7–10]. In [7], the dynamical intricacies of a single-species discrete population model with stage structure and birth pulses were examined. Liu *et al.* [8] suggested an impulsive control method for controlling bifurcations and chaos in an internet congestion control system. In [9,10], Jiang *et al.* explored the intricate dynamics of the Logistic map through the incorporation of periodic impulsive forces. It is noted that the above studies are all for the discrete systems with periodic impulsive forces, but to the best of our knowledge, there have been limited investigations on the discrete systems subject to state-dependent impulsive forces. However, the impulsive forces usually depend on the states of the discrete systems in engineering applications. This paper aims to gain an in-depth insight into the discrete systems with state-dependent impulsive forces by using the Logistic map as an example and studying how the state-dependent impulsive force affects its dynamics.

Robert May initially examined the Logistic map in [11], which is a straightforward quadratic map exhibiting diverse dynamics, and it has been extensively examined by various researchers in subsequent studies across different fields, including population projection, environmental ecology, and secure messaging [12–14]. In [14], Bischi *et al.* examined the dynamics of a fishery model that incorporates a non-continuous on-off harvesting strategy into a Logistic model. Indeed, the Logistic map involving impulsive forces is a discontinuous map where one may come across border-collision bifurcation (BCB). When an invariant set (e.g., a fixed point or a periodic orbit), meets a discontinuity boundary, BCB will happen, and there could be a significant alteration in its overall behavior, such as shifting from a fixed point to a periodic orbit or a chaotic attractor [15,16]. Feigen [15] initially examined and referred to the C-bifurcation as BCB while exploring the bifurcations in piecewise smooth systems. Subsequently, Nusse and Yorke [16] coined the phrase BCB to describe the bifurcations linked to the boundary points. The literature has documented reports on BCB in one-, two-, three- and n- dimensional piecewise smooth systems [17–26]. In [21], Gardini *et al.* investigated the codimension-2 border-collision bifurcations in one-dimensional discontinuous piecewise smooth maps. In [22], Avrutin *et al.* studied various invariant sets and bifurcation structures of a class of one-dimensional piecewise monotone maps defined on two partitions. Panchuk *et al.* investigated the bifurcation phenomenon, including BCB of a class of two-dimensional non-smooth maps using the first return map in [26].

Very recently, nonlinear maps, including memristive maps, have received much attention since their broad applications [27–31]. In [27], Muni and Banerjee presented some three-dimensional maps to illustrate bifurcation scenarios of mode-locked periodic orbits and the closed invariant curves. Bao et al. examined the initial-dependent dynamics of a class of there-dimensional memristive maps in [28]. In [29], Li et al. explored the complex dynamic behaviors of a class of memristive Rulkov maps. Bao et al. demonstrated the complex dynamics of a class of two-dimensional memristive maps under the sine transform in [30]. In [31], Li et al. studied the problem of offset boosting and controllability of nonlinear maps.

This paper aims to investigate the complex behavior of the Logistic map, which experiences impulsive perturbations dependent on its state. The main contributions of this paper are as follows: (1) The mathematical model of the Logistic map involving impulsive forces is presented. (2) The BCB of periodic orbits is examined by creating the two-parameter bifurcation diagrams of the map. (3) Several bifurcation scenarios related to the existence of BCB are demonstrated.

The remaining portion of this document is organized in the following manner. In Section 2, we formulate the mathematical model of the Logistic map with state-dependent impulsive forces. In Section 3, the conditions of stability and BCB of periodic orbits are given. In Section 4, one- and two-parameter bifurcation diagrams of the Logistic map with state-dependent impulsive forces are presented, and several bifurcation scenarios related to the BCB of periodic orbits are investigated. In Section 5, several findings are presented.

2. System model

Consider the Logistic map written as the following difference equation

$$x(k+1) = rx(k)(1-x(k)) \tag{1}$$

where $x(k) \in [0,1]$ $(k = 0, 1, 2, ...)$ denotes the system state and r is a system parameter.

Assuming that the Logistic map (1) is disturbed by an impulsive force when its state x is less than the fixed value h, we can express the difference equation of the Logistic map perturbed by the state-dependent impulsive force as

$$\begin{cases} x(k+1) = rx(k)(1-x(k)) & x(k) > h, \\ \Delta x(k+1) = x(k+1) - x(k) = \alpha & x(k) \le h, \end{cases} \tag{2}$$

where $0 < h < 1$ and $0 < \alpha < 1 - h$ determine the strength of the impulsive force. The system (2) can be written as

$$\begin{cases} x(k+1) = rx(k)(1-x(k)) & x(k) > h, \\ x(k+1) = x(k) + \alpha & x(k) \le h. \end{cases} \tag{3}$$

The system (3) contains one breakpoint, but it is not continuous at this breakpoint, which is different from the system studied in [17].

3. Fixed points and periodic orbits

Denoting $f^R(x)$ as $rx(1-x)$ and $f^L(x)$ as $x+\alpha$, we can differentiate $f^R(x)$ and $f^L(x)$ with respect to x as $f_x^R(x) = r(1-2x)$ and $f_x^L(x) = 1$, respectively. We use R (if $x_i > h$) and L (if $x_i \le h$) as the symbolic representations of the period-n orbit with periodic points x_1, x_2, $\cdots$, x_n. For example, a

period-3 orbit with periodic points $x_1 \leq h$, $x_2 > h$, and $x_3 > h$ can be represented by LR^2. This section focuses on examining fixed points and periodic orbits of the system (3).

When $x \leq h$, there is no solution for the equation $x = f^L(x) = x + \alpha$ if $\alpha > 0$, so any fixed point does not exist. When $x > h$, from $x = f^R(x) = rx(1-x)$, we can obtain either $x = 0$ or $x = 1 - \frac{1}{r}$. When $x = 1 - \frac{1}{r} > h$, i.e. $r > \frac{1}{1-h}$, there is a fixed point $x^* = 1 - \frac{1}{r}$. Since $f_x^R(x^*) = 2 - r$, it can be inferred that the fixed point x^* is stable when $\frac{1}{1-h} < r < 3$. At $r = 3$, $f_x^R(x^*) = 2 - r = -1$, so the fixed point x^* becomes unstable, and a period-2 orbit emerges via a period-doubling bifurcation. By applying the formula $x = (f^R)^{(2)}(x) = f^R(f^R(x))$, we can derive the period-2 points, $x^{**}(1)$ and $x^{**}(2)$. As the parameter r increases, a period-4 orbit may exist through the period-doubling bifurcation followed by a cascade of period-doubling bifurcations resulting in chaos. Fig.1 (a) depicts the bifurcation diagram of the Logistic map with state-dependent impulsive forces calculated for $r \in [1.25, 4]$ with $h = 0.2$ and $\alpha = 0.4$, and Fig. 1 (b) displays the bifurcation diagram of the Logistic map without state-dependent impulsive forces. From Fig. 1, the dynamics of the Logistic map with state-dependent impulsive forces is the same as the one without state-dependent impulsive forces if the trajectory does not go across the discontinuity boundary $x = h$. However, when one point of the trajectory goes across the discontinuity boundary $x = h$, the inconsistency of the dynamics, e.g., the length of periodic windows and the chaotic range, occurs.

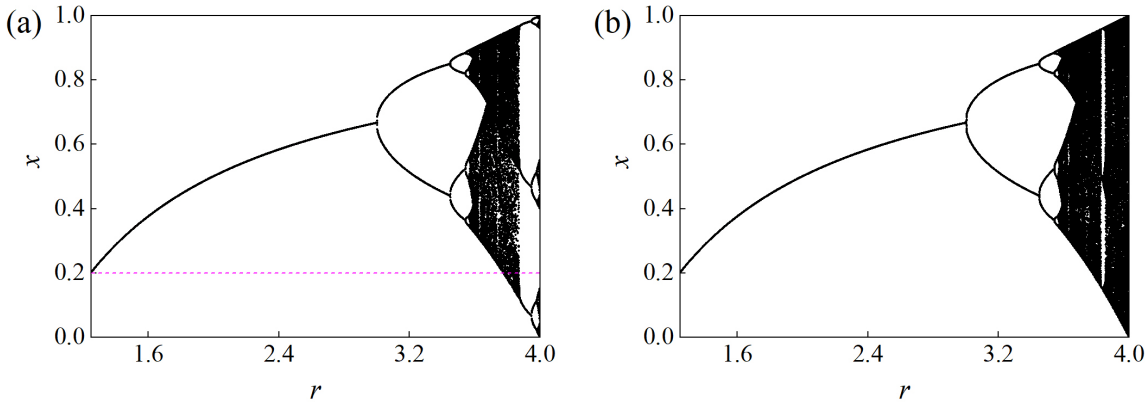

Fig. 1. (Colour online) One-parameter bifurcation diagrams of the Logistics map (a) with and (b) without state-dependent impulsive forces calculated for $r \in [1.25, 4]$, $h = 0.2$, $\alpha = 0.4$. The discontinuity boundary $x = 0.2$ is marked by a dashed magenta line.

There are many types of periodic orbits for specific parameters. Firstly, we consider the period-2 orbit with the symbolic representation LR. Suppose that x_L^*, x_R^* are periodic points, from $x_L^* = f^R(x_R^*)$ and $x_R^* = f^L(x_L^*)$, we have $x_L^* = f^R(f^L(x_L^*))$ and the stability condition can be written as

$$|f_x^R(f^L(x_L^*)) \times (f_x^L(x_L^*))| < 1$$

The BCB happens when a periodic point comes into contact with the discontinuity boundary. Since

the Logistic map is quadratic, finding a general analytical expression for the periodic orbits is difficult. However, the proposed method can be employed to numerically determine the existence, stability, and BCB of the periodic orbits, e.g., Newton's method [32].

For example, we can consider the period-n orbit with the symbolic representation LR^{n-1}, which is called the primal periodic orbit, and its periodic points are given as x_1, x_2, $\cdots$, x_n, where $x_1 \leq h$ and $x_i > h$, $i = 2, \cdots, n$. The existence condition of this orbit can be expressed as $x_2 = f^L(x_1)$, $x_3 = f^R(x_2)$, $\cdots$, $x_n = f^R(x_{n-1})$, and $x_1 = f^R(x_n)$. The stability condition can be written as

$$|f_x^R(x_n) \times \cdots \times f_x^R(x_2) \times f_x^L(x_1)| = |f_x^R(x_n) \times \cdots \times f_x^R(x_2)| < 1$$

When a periodic point touches the discontinuity boundary $x = h$, it will result in BCB.

Likewise, for the period-n orbit with the symbolic representation $L^{n-1}R$ which is also known as the primal periodic orbit, and its periodic points are written as x_1, x_2, $\cdots$, x_n, where $x_i \leq h$ and $x_n > h$, $i = 1, \cdots, n-1$. The existence condition of this orbit can be expressed as $x_2 = f^L(x_1)$, $x_3 = f^L(x_2)$, $\cdots$, $x_n = f^R(x_{n-1})$, and $x_1 = f^L(x_n)$. The stability condition can be written as

$$|f_x^R(x_n) \times f_x^L(x_{n-1}) \cdots \times f_x^L(x_2) \times f_x^L(x_1)| = |f_x^R(x_n)| < 1$$

When a periodic point touches the discontinuity boundary $x = h$, it will result in BCB.

The following section will conduct numerical simulations for the periodic orbits and study their different bifurcation scenarios in detail.

4. Bifurcation of periodic orbits

4.1. Bifurcation structure

To demonstrate the complex dynamics of the system (3) concerning the parameters, the so-called "following the attractor" method [33] was used to generate the dynamical regions. The dynamical regions of the system (3) in the parameter plane (r, α) calculated for $h = 0.2$ are presented in Fig. 2, where Fig. 2(a) and (b) show the dynamical regions calculated as the branching parameters increase and decrease, respectively. Different colors mark the regions of different stable periodic orbits, and the regions of these orbits are usually called periodicity regions (or periodicity tongues according to their shapes). The regions of the periodic orbit whose period is larger than 16 and the chaotic orbit are indicated by grey. The following study will focus on three special bifurcation scenarios marked by A, B, and C in Fig. 2. In the region of A, period-2 and period-4 orbits are recorded, and they may coexist with a fixed point. The period increment scenario with coexisting attractors is observed in the region of B. The period-adding scenario without coexisting attractors is recorded in the region of C. Since BCB exists, the phenomena of coexisting attractors take place. The coexisting attractors can usually be found by increasing and decreasing branching parameters. Thus, the system (3) exhibits different dynamics in some regions containing coexisting attractors in Fig. 2.

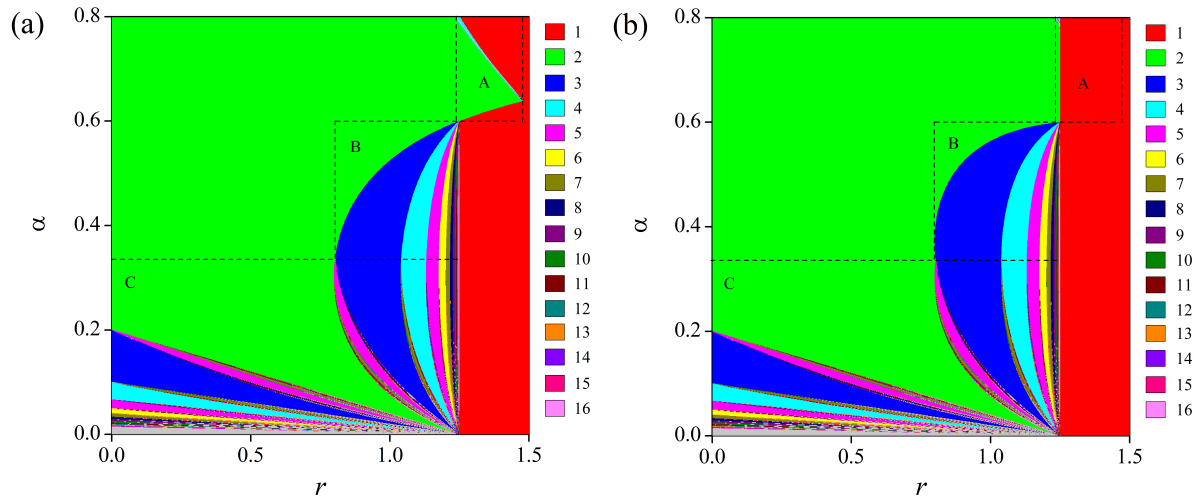

Fig. 2. (Colour online) Dynamical regions of the system (3) in the parameter plane (r, α) calculated for $h = 0.2$ by numerical simulations as the branching parameters (a) increase or (b) decrease. Different colors indicate the regions for different periodic orbits, and the number of periods can be referred to as the numbers listed in the legend. The regions for the periodic orbit whose period is larger than 16 and the chaotic orbit are shown in grey.

4.2. Period-doubling bifurcation with coexisting attractors

The one-parameter bifurcation diagram of the system (3) by varying the parameter $r \in [0, 1.5]$ and keeping the parameters $h = 0.2$, $\alpha = 0.75$ is shown in Fig. 3(a), and a zoom up of the bifurcations in the shaded area of Fig. 3(a) is presented in Fig. 3(b). From Fig. 3, a period-2 orbit with the symbolic representation LR is recorded for $r \in [0, 1.303)$. The period-4 orbit with the symbolic representation $LRLR$ occurs through a period-doubling bifurcation when r equals 1.303. As the parameter r increases, the period-4 orbit ends at $r = 1.312$ due to a border-collision bifurcation. A fixed point is recorded for $r \in [1.25, 1.5]$, which coexists with the period-2 and the period-4 orbits for $r \in [1.25, 1.312)$. As the parameter r decreases, the border-collision bifurcation of the fixed point can be observed when r equals 1.303. Fig. 4 depicts the Cobweb diagrams of the period-2 orbit at $r = 1.25$ and the period-4 orbit at $r = 1.305$.

Fig. 5 presents the bifurcation diagrams of the system (3) by varying the parameter r within the range of $[0, 1.5]$ and fixing the parameters $h = 0.2$, $\alpha = 0.6$ and $\alpha = 0.64$. Fig. 5(b) shows that the period-2 orbit disappears at $r = 1.477$ via a BCB, and the fixed point is left. The fixed point coexists with the period-2 orbit for $r \in [1.25, 1.477)$. As the parameter α decreases, this coexistence regime entirely disappears, as shown in Fig. 5(a), so that only a BCB from the period-2 orbit to the fixed point is observed.

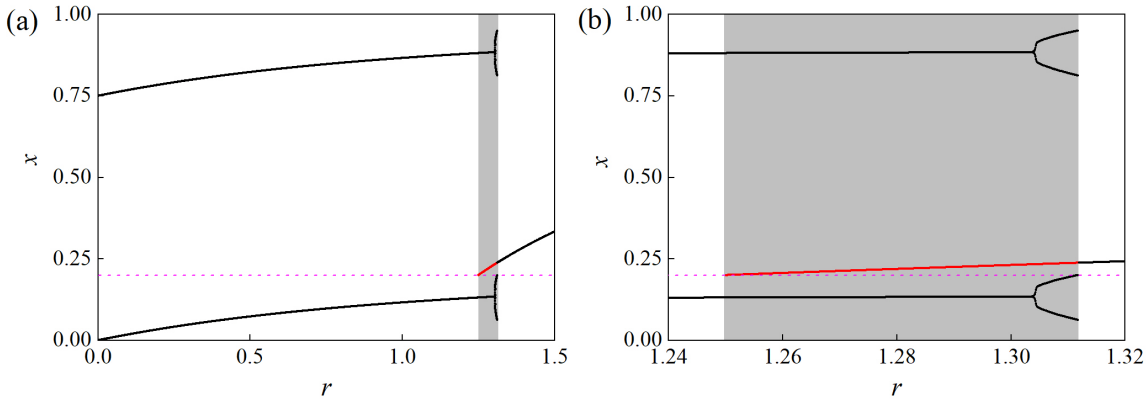

Fig. 3. (colour online) (a) One-parameter bifurcation diagram of the system (3) constructed for varying the parameter $r \in [0, 1.5]$, and $h = 0.2$, $\alpha = 0.75$. (b) One-parameter bifurcation diagram in the shaded range in Fig. 3(a). The discontinuity boundary $x = 0.2$ is marked by a dashed magenta line, and red dots show coexisting attractors.

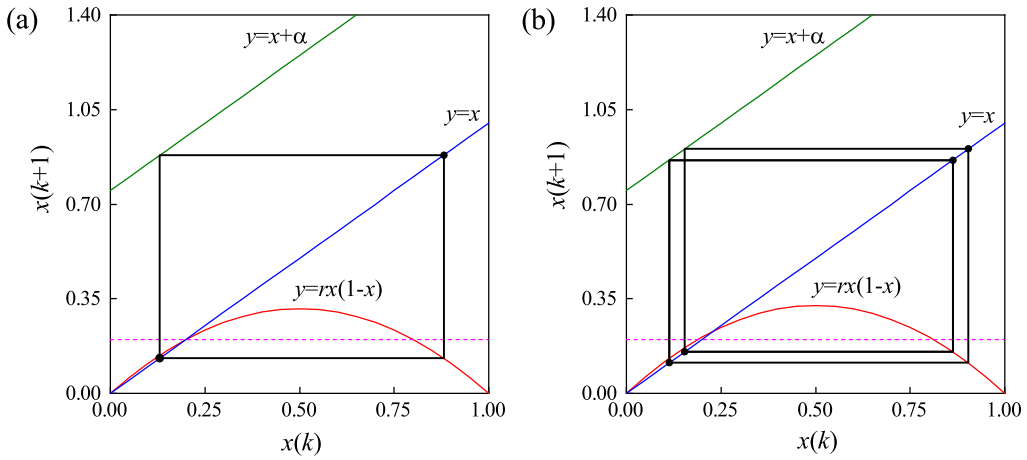

Fig. 4. (colour online) Cobweb diagrams showing the iterates of the system (3) calculated for $h = 0.2$, $\alpha = 0.75$, (a) $r = 1.25$, and (b) $r = 1.305$. The discontinuity boundary $x = 0.2$ is shown by a dashed magenta line.

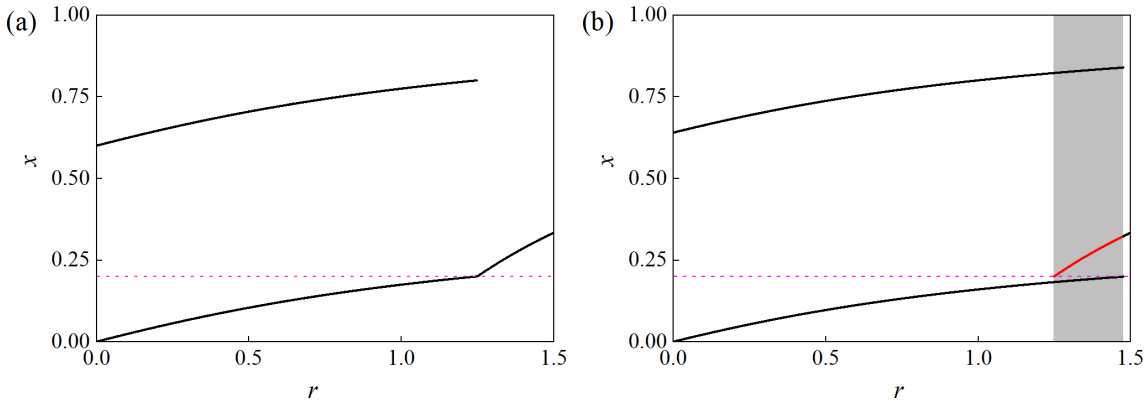

Fig. 5. (colour online) One-parameter bifurcation diagram of the system (3) constructed for varying the parameter $r \in [0, 1.5]$, and $h = 0.2$, (a) $\alpha = 0.6$, (b) $\alpha = 0.64$. The discontinuity boundary $x = 0.2$ is marked by a dashed magenta line, and red dots show coexisting attractors.

4.3. Period increment scenario with coexisting attractors

The period increment scenario with coexisting attractors is recorded in the region of B in Fig. 2. Such bifurcation is illustrated in Fig. 6 by varying the parameter r within $[0, 1.5]$ while keeping the parameter h at 0.2 and the parameter α at 0.4. Fig. 6 displays some regions where two periodic orbits coexist. For $r \in [0, 0.833]$, the system (3) exhibits a period-2 orbit with the symbolic representation LR. The Cobweb diagram of the period-2 orbit calculated for $r = 0.4$ is presented in Fig. 7(a), where one of the points is above the discontinuity boundary $x = h$ while another one is below. As the parameter r increases, the periodic point below intersects with the boundary at $r = 0.833$ from the left side, resulting in a BCB. As a result, the period-2 orbit vanishes, leaving behind the period-3 orbit with the symbolic representation LRR. The Cobweb diagram of the period-3 orbit calculated for $r = 0.9$ is given in Fig. 7(b), and it can be seen that two periodic points are above the boundary $x = h$ while one periodic point is below. The value of r decreases until it reaches 0.803, causing one of the fixed points to collide with the boundary and resulting in the disappearance of the period-3 orbit. Therefore, the period-2 and the period-3 orbit coexist for $r \in [0.803, 0.833]$. The same dynamical phenomena are observed in Fig. 7(c) and (d), such that once the periodic point below the boundary $x = h$ collides with the boundary, one additional periodic point emerges.

As the parameter r increases in Fig. 6, the period-3 orbit with the symbolic representation LR^2 experiences a BCB at $r = 1.141$, resulting in the emergence of a period-4 orbit with the symbolic representation LR^3. As the parameter r decreases, the period-4 orbit undergoes a BCB at $r = 1.047$. So the period-3 and the period-4 orbits coexist for $r \in [1.047, 1.141]$. Repeating the same bifurcation scenario, the BCB causes the period-i ($i \geq 3$) orbit to disappear, and a coexisting period-$(i + 1)$ orbit is left as the parameter r increases. On the other hand, the BCB results in the disappearance of the

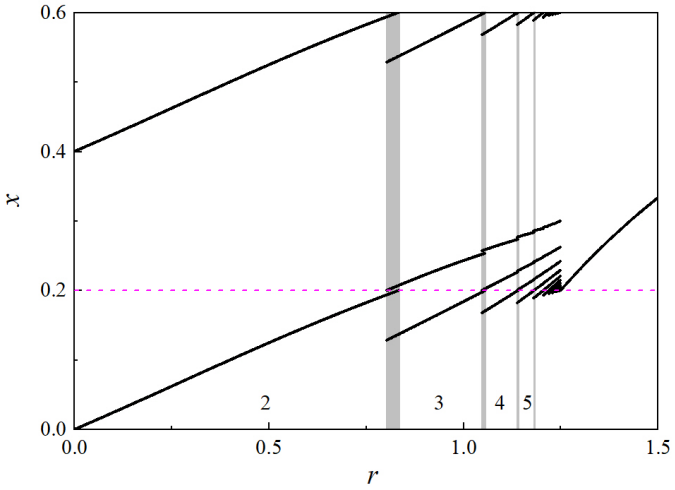

Fig. 6. (colour online) One-parameter bifurcation diagram of the system (3) constructed for varying the parameter $r \in [0, 1.5]$, and $h = 0.2$, $\alpha = 0.4$. The discontinuity boundary $x = 0.2$ is marked by a dashed magenta line, and coexistence regions are shaded by grey. The numbers in the figure indicate the period of the periodic solutions.

period-i orbit, and a coexisting period-$(i-1)$ orbit is left as the parameter r decreases. This iteration will continue until the parameter r reaches $r = \frac{1}{1-h} = 1.25$ where the system (3) has a stable fixed point at $x = 1 - \frac{1}{r} = h$.

4.4. Period-adding scenario

The period-adding scenario is recorded in the region of C in Fig. 2, and one of the bifurcations is shown in Fig. 8(a) by varying the parameter $r \in [0, 1.5]$ and fixing the parameters $h = 0.2$, $\alpha = 0.05$. No coexisting periodic orbit is observed in Fig. 8(a), and the period-adding regions are marked in grey. The perio-adding scenario terminates at $r = \frac{1}{1-h} = 1.25$ where the system (3) only has a stable fixed point $x = 1 - \frac{1}{r} = h$. The iterates of the system (3) using Cobweb diagrams for $\alpha = 0.05$ are presented in Fig. 9. It can be seen from Fig. 9 that as the parameter r increases, one of the attractors collides with the discontinuity boundary $x = h$. The primary periodic orbit evolves from L^4R to LR.

Fig. 8(b) presents the period-adding scenario calculated for $\alpha = 0.2$, and the same period-adding scenarios are observed in the grey area. Fig. 10 shows the iterates of the system (3) using Cobweb diagrams for $\alpha = 0.2$. As the parameter r increases, the primary periodic orbit changes from LR to LR^4 via the BCB. Again, infinite period orbits and period-adding scenarios exist before the primary period-1 orbit is encountered. Summarizing from the above studies, we can conclude that period-$(k_1 + k_2)$ orbits occur between the primary period-k_1 and period-k_2 orbits in the regime of C.

From Figs. 6 and 8, there are differences between the period increment scenario and the period-adding scenario. The period increment scenario is associated with coexisting attractors. The shaded grey

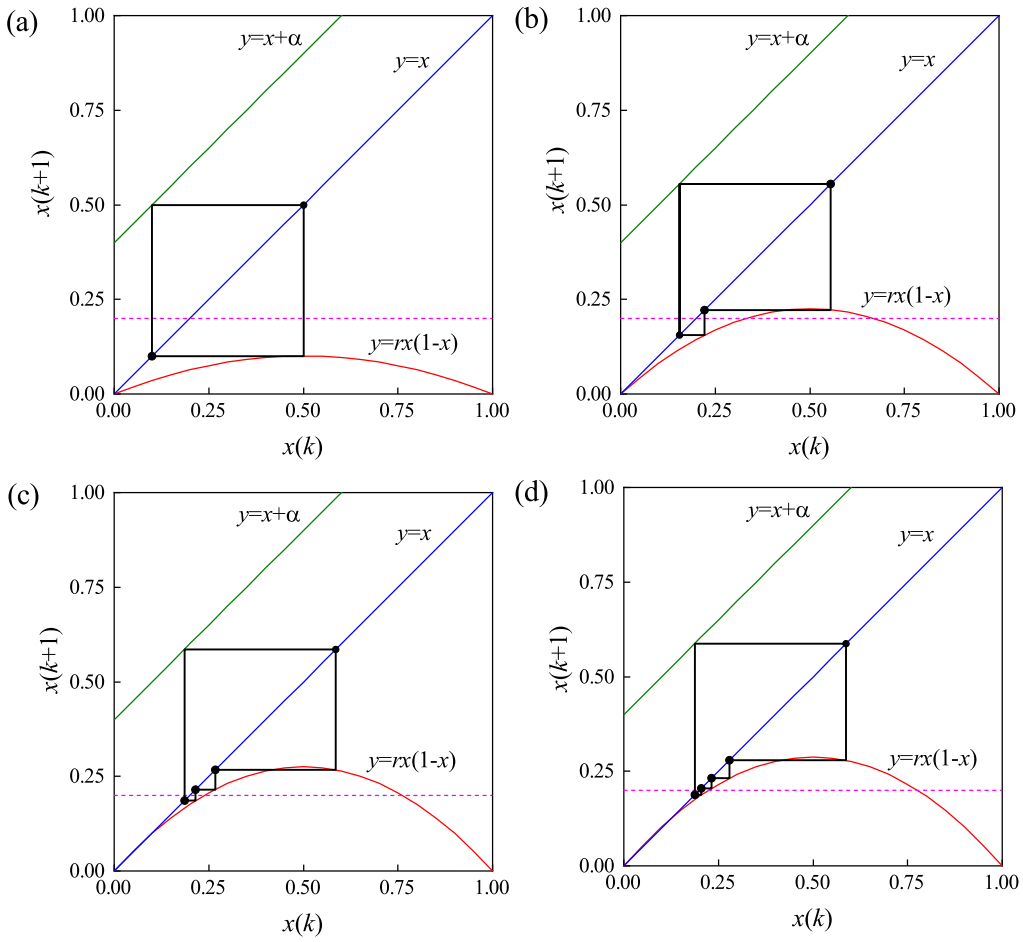

Fig. 7. (colour online) Cobweb diagrams showing the iterates of the system (3) calculated for $h = 0.2$, $\alpha = 0.4$, (a) $r = 0.4$, (b) $r = 0.9$, (c) $r = 1.1$, and (d) $r = 1.15$. The discontinuity boundary $x = 0.2$ is shown by a dashed magenta line.

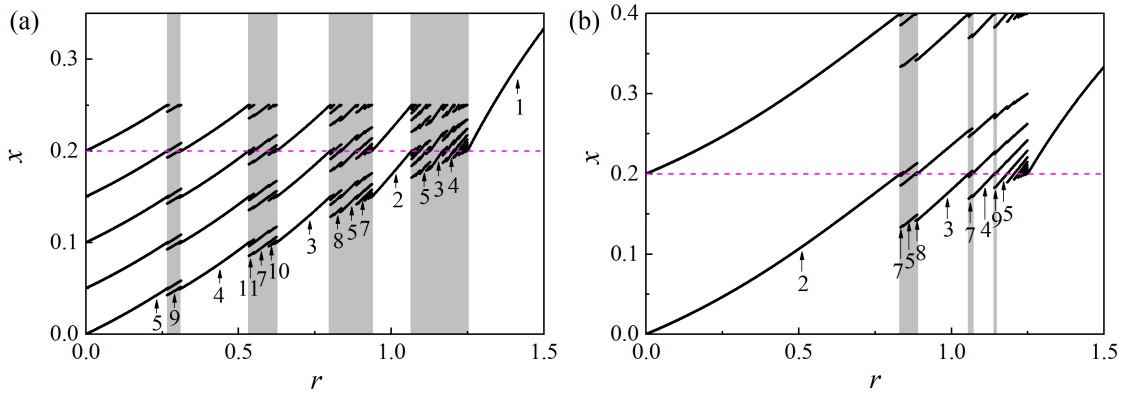

Fig. 8. (colour online) One-parameter bifurcation diagram of the system (3) constructed by varying the parameter $r \in [0, 1.5]$, and $h = 0.2$, (a) $\alpha = 0.05$, (b) $\alpha = 0.20$. A dashed magenta line marks the discontinuity boundary $x = 0.2$, and period-adding regions are shaded by grey.

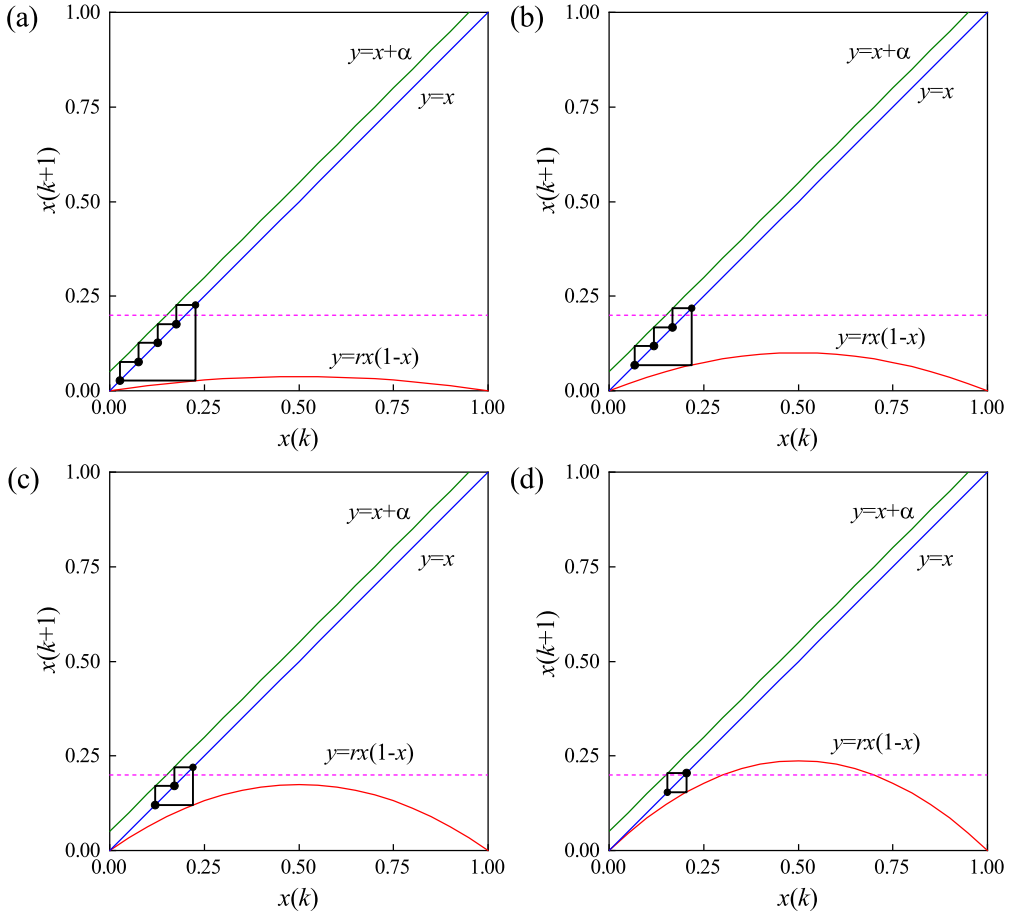

Fig. 9. (colour online) Cobweb diagrams showing the iterates of the system (3) calculated for $h = 0.2$, $\alpha = 0.05$, (a) $r = 0.15$, (b) $r = 0.4$, (c) $r = 0.7$, and (d) $r = 0.95$. The discontinuity boundary $x = 0.2$ is shown by a dashed magenta line.

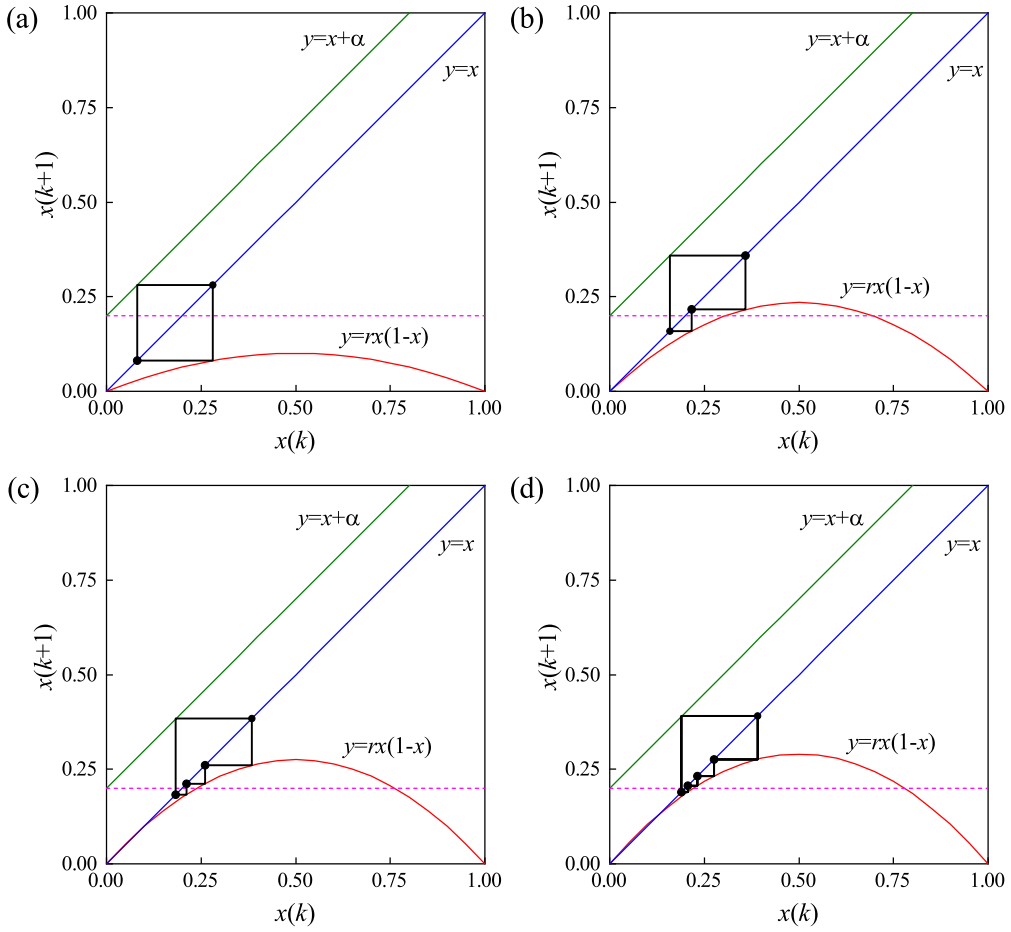

Fig. 10. (colour online) Cobweb diagrams showing the iterates of the system (3) computed for $h = 0.2$, $\alpha = 0.2$, (a) $r = 0.4$, (b) $r = 0.94$, (c) $r = 1.1$, and (d) $r = 1.16$. The discontinuity boundary $x = 0.2$ is shown by a dashed magenta line.

in Fig. 6 denotes the coexistence regions where two periodic orbits coexist. However, the period-adding scenario is not related to coexisting attractors. The shaded grey in Fig. 8 denotes the period-adding regions where new periodic orbits exist.

4.5. Bifurcation curves

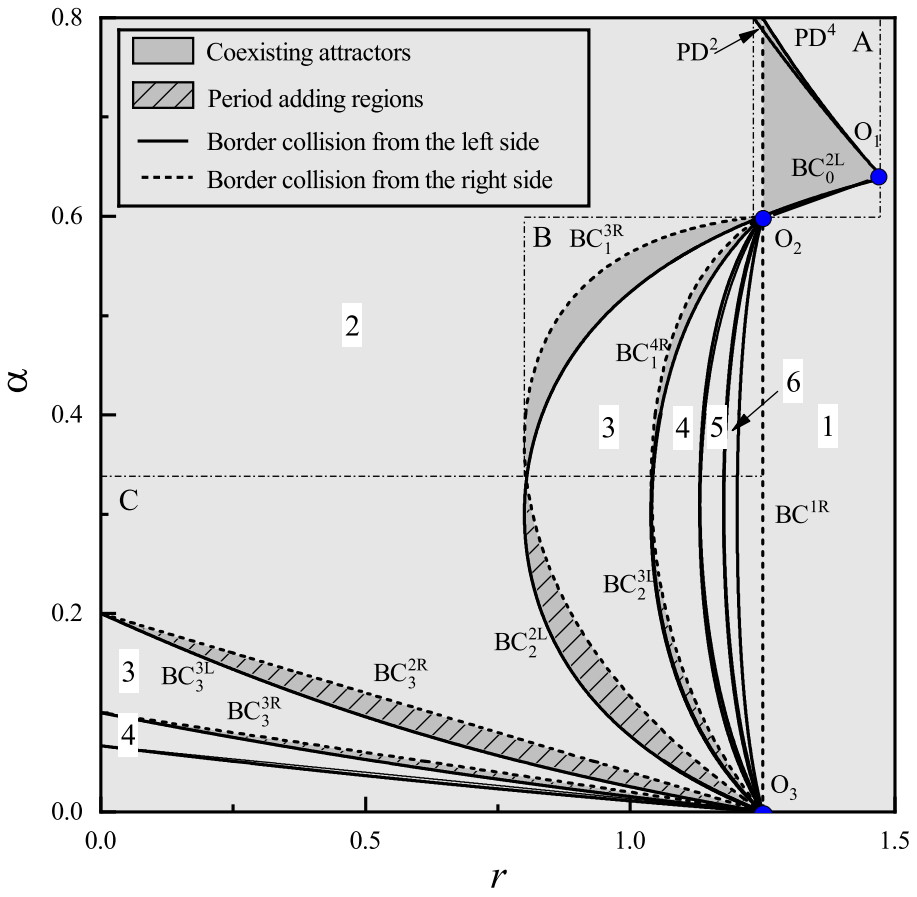

Fig. 11. (colour online) Two-parameter bifurcation diagram of the system (3) in the parameter plane (r, α) computed for $h = 0.2$.

By following the bifurcation points recorded in the previous sections, a number of bifurcation curves of the periodic orbits in the low period are calculated by using Newton's method [32] and depicted in Fig. 11. For simplicity, we use the abbreviations in the two-parameter bifurcation diagram to describe different bifurcation curves, e.g. BC_1^{2R} represents the initial border-collision curve for the period-2 orbit from the right side, PD^2 illustrates the period-doubling curve for the fixed point, PD^4 represents the period-doubling curve for the period-2 orbit. As can be seen from Fig. 11 that, there are three particular bifurcation points O_1, O_2, and O_3, where O_1 is the intersection point of PD^2, PD^4, and BC^{2L}, O_2 is the intersection point of BC_0^{2L}, BC^{1R}, BC_1^{3R}, BC_2^{2L}, BC_1^{4R}, BC_2^{3L} ..., BC_1^{kR}, $BC_2^{(k-1)L}$ and BC^{1R}, and O_3

is the intersection point of BC_3^{kL}, $BC_3^{(k-1)R}$, ..., BC_3^{3L}, BC_3^{2R}, BC_2^{2L}, BC_1^{3R}, ..., $BC_2^{(k-1)L}$, BC_1^{kR}, and BC_2^{1R}. The codimension-2 border-collision bifurcation points O_2 and O_3 known as organizing centers in [19, 21] were defined as the bifurcation points from which an infinite number of bifurcation curves originate. Note that the two-parameter bifurcation diagram in Fig.11 matches the dynamical regions presented in Fig. 2.

5. Conclusions

This paper explores the intricate dynamics of the Logistic map involving impulsive forces that depend on the state. The conditions of stability and BCB of periodic orbits have been presented. To demonstrate the significance of the BCB of the system, we have created the dynamical regions and the bifurcation diagram with two parameters. The bifurcation curves for the periodic orbits in the low period have been computed to elucidate the corresponding bifurcation scenarios, encompassing the period-doubling bifurcation, period increment scenario, and period-adding scenario. The potential applications of the Logistic map involving impulsive forces include data, image, and video encryption. Future work will study the complex dynamics of high-dimensional maps with impulsive forces and their applications.

Acknowledgements

The authors would like to thank the anonymous reviewers for their valuable suggestions that have improved the overall quality of the paper.

References

[1] M. A. Bayrak and A. Demir, On the challenge of identifying space dependent coefficient in space-time fractional diffusion equations by fractional scaling transformations method, *Turkish J. Science*, **7** (2022), 132-145.

[2] A. A. Tunik, O. A. Sushchenko, S. I. Ilnytska and V. M. Kondratiuk, Determination of the quadrotor mathematical models for control systems synthesis and simulation, *Appl. Comput. Math.*, **22** (2023), 116-132.

[3] T. Yang, *Impulsive control theory*. Springer, Berlin, 2001.

[4] J. J. Yu, H. B. Jiang, C. G. Zhou and L. P. Zhang, Delay-dependent exponential stabilization of nonlinear fuzzy impulsive systems with time-varying delay, *Neurocomputing*, **203** (2016), 92-101.

[5] X. B. Rao, X. P. Zhao, Y. D. Chu, J. G. Zhang and J. S. Gao, The analysis of mode-locking topology in an SIR epidemic dynamics model with impulsive vaccination control: Infinite cascade of Stern-Brocot sum trees, *Chaos Solit. Fract.*, **139** (2020), 110031.

[6] I. U. Khan and S. Tang, The impulsive model with pest density and its change rate dependent feedback control, *Discrete Dyn. Nat. Soc.*, **2020** (2020), 4561241.

[7] S. J. Gao and L. S. Chen, Dynamic complexities in a single-species discrete population model with stage structure and birth pulses, *Chaos Solit. Fract.*, **23** (2005), 519-527.

[8] F. Liu, Z. H. Guan and H. O. Wang, Controlling bifurcations and chaos in TCP-UDP-RED, *Nonlinear Anal. Real World Appl.*, **11** (2010), 1491-1501.

[9] H. B. Jiang, T. Li, X. L. Zeng and L. P. Zhang, Bifurcation analysis of complex behavior in the Logistic map via periodic impulsive force, *Acta Phys. Sin.*, **62** (2013), 120508. (in Chinese).

[10] H. B. Jiang, T. Li, X. L. Zeng and L. P. Zhang, Bifurcation analysis of the Logistic map via two periodic impulsive forces, *Chin. Phys. B*, **23** (2014), 010501.

[11] R. M. May, Simple mathematical models with very complicated dynamics, *Nature*, **261** (1976), 459-467.

[12] T. Nagatani and N. Sugiyama, Vehicular traffic flow through a series of signals with cycle time generated by a logistic map, *Phys. A*, **392** (2013), 851-856.

[13] X. Y. Wang, N. Guan and J. J. Yang, Image encryption algorithm with random scrambling based on one-dimensional logistic self-embedding chaotic map, *Chaos Solit. Fract.*, **150** (2021), 111117.

[14] G. I. Bischi, F. Lamantia and F. Tramontana, Sliding and oscillations in fisheries with on-off harvesting and different switching times, *Commun. Nonlinear Sci. Numer. Simul.*, **19** (2014), 216-229.

[15] M. I. Feigin, Doubling of the oscillation period with C-bifurcations in piecewise-continuous systems, *J. Appl. Math. Mech.*, **34** (1970), 822-830.

[16] H. E. Nusse and J. A. Yorke, Border-collision bifurcations including period two to period three for piecewise smooth systems, *Phys. D*, **57** (1992), 39-57.

[17] I. Sushko, A. Agliari and L. Gardini, Bifurcation structure of parameter plane for a family of unimodal piecewise smooth maps: Border-collision bifurcation curves, *Chaos Solit. Fract.*, **29** (2006), 756-770.

[18] G. I. Bischi, L. Gardini and U. Merlone, Impulsivity in binary choices and the emergence of periodicity, *Discrete Dyn. Nat. Soc.*, **2019** (2009), 407913.

[19] I. Sushko, L. Gardini and K. Matsuyama, Superstable credit cycles and U-sequence, *Chaos Solit. Fract.*, **59** (2014), 13-27.

[20] V. Avrutin, L. Gardini, M. Schanz and I. Sushko, Bifurcations of chaotic attractors in one-dimensional piecewise smooth maps, *Int. J. Bifurc. Chaos*, **24** (2014), 1440012.

[21] L. Gardini, V. Avrutin and I. Sushko, Codimension-2 border collision bifurcations in one-dimensional discontinuous piecewise smooth maps, *Int. J. Bifurc. Chaos*, **24** (2014), 1450024.

[22] V. Avrutin, L. Gardini, I. Sushko and F. Tramontana, *Continuous and discontinuous piecewise-smooth one-dimensional maps: invariant sets and bifurcation structures*. World Scientific, Singapore, 2019.

[23] D. J. W. Simpson, Unfolding codimension-two subsumed homoclinic connections in two-dimensional piecewise-linear maps, *Int. J. Bifurc. Chaos*, **30** (2020), 2030006.

[24] E. G. Gu, Multistability regions and related basins of multiattractors in piecewise linear discontinuous map from financial markets, *Int. J. Bifurc. Chaos*, **31** (2021), 2150107.

[25] M. Patra, S. Gupta and S. Banerjee, Local and global bifurcations in 3D piecewise smooth discontinuous maps, *Chaos*, **31** (2021), 013126.

[26] A. Panchuk, I. Sushko, E. Michetti and R. Coppier, Revealing bifurcation mechanisms in a 2D nonsmooth map by means of the first return map, *Commun. Nonlinear Sci. Numer. Simul.*, **117** (2023), 106946.

[27] S. S. Muni and S. Banerjee, Bifurcations of mode-locked periodic orbits in three-dimensional maps, *Int. J. Bifurc. Chaos*, **33** (2023), 2330025.

[28] H. Bao, Z. Hua, H. Li, M. Chen and B. Bao, Memristor-based hyperchaotic maps and application in auxiliary classifier generative adversarial nets, *IEEE Trans. Ind. Inf.*, **18** (2022), 5297-5306.

[29] K. Li, H. Bao, H. Li, J. Ma, Z. Hua and B. Bao, Memristive Rulkov neuron model with magnetic induction effects, *IEEE Trans. Ind. Inf.*, **18** (2022), 1726-1736.

[30] H. Bao, H. Li, Z. Hua, Q. Xu and B. Bao, Sine-transform-based memristive hyperchaotic model with hardware implementation, *IEEE Trans. Ind. Inf.*, **19** (2023), 2792-2801.

[31] C. Li, C. Yi, Y. Li, S. Mitro and Z. Wang, Offset boosting in a discrete system, *Chaos*, **34** (2024), 031102.

[32] D. Ito, T. Ueta, T. Kousaka and K. Aihara, Bifurcation analysis of the Nagumo-Sato model and its coupled systems, *Int. J. Bifurc. Chaos*, **26** (2016), 1630006.

[33] J. A. C Gallas, The role of codimension in dynamical systems, *Int. J. Mod. Phys. C*, **3** (1992), 1295-1321.

E-mail address: yctcjhb@126.com

E-mail address: y.liu2@exeter.ac.uk

E-mail address: yctczlp@126.com

E-mail address: yujianjiang@126.com